DESIGN AND INVESTIGATION OF A CONTRA-ROTATING CENTRIFUGAL FAN

Christian FRIEBE[1], Oliver VELDE[2],
Karsten HACKESCHMIDT[1]

[1] *Institut für Luft- und Kältetechnik gGmbH, Bertolt-Brecht-Allee 20, 01309 Dresden, Germany*

[2] *CFturbo GmbH, Unterer Kreuzweg 1, 01097 Dresden, Germany*

SUMMARY

In this approach we present the results and outcomes of the design process and the experimental examination of a contra-rotating centrifugal fan comprising two concentrically rotating impellers and two drives. The fan is designed for a volume flow of 150 m^3h^{-1} and 205 *Pa* (static pressure). The diameter is 150 *mm* and the rotational speed of the inner impeller (impeller A) and the outer impeller (Impeller B) is 3000 *rpm* and 1500 *rpm*, respectively.

INTRODUCTION

Centrifugal fans are common in many fields of application. A centrifugal fan consists of a drive, an impeller, and a volute [1]. The volute is designed to convert the dynamic pressure at the outlet of the fan impeller into static pressure and to guide the flow towards a connected geometry, e.g. a duct. However, centrifugal fans without a volute are being used more and more often [2]. A common application is the installation in an air conditioning unit, where typically the dynamic pressure at the outlet is dissipated. In this way, both manufacturing costs and installation space can be saved. On the other hand it must be noted that the air at the outlet of the fan is strongly swirled, which may lead to inadequate acoustic and aerodynamic behaviour of subsequent devices (see fig. 1). These two disadvantages of a fan without casing led to the consideration of a contra-rotating fan. The advantages of a contra-rotating fans are well known and examined for axial fans [3]–[8], but rarely investigated for centrifugal fans [9], [10].

WORKING PRINCIPLE

The working principle of a centrifugal fan without volute is based on the deceleration of a an air stream velocity $\boldsymbol{w}$ within an impeller from inlet (1) to outlet (2) according to fig. 2 (top). This velocity-

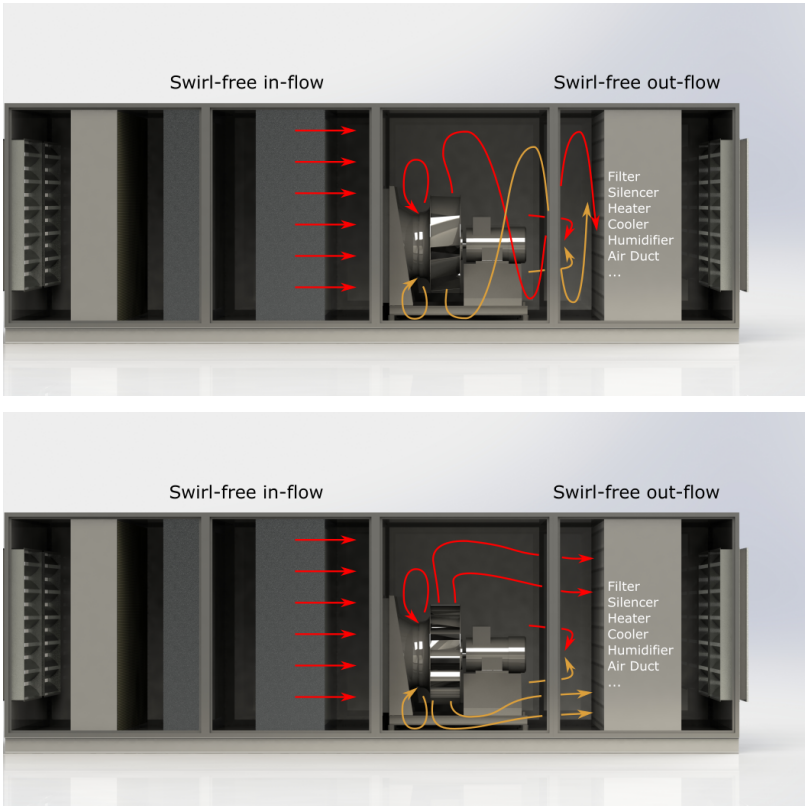

Figure 1: Typical flow conditions in an Air Handling Unit top: centrifugal fan without volute, bottom: contra-rotating centrifugal fan

vector $\boldsymbol{w}$ represents the air velocity of the rotating coordinate-system of the impeller and depends upon the inlet velocity $\boldsymbol{c}$ of the non-rotating coordinate-system and the circumferential speed $\boldsymbol{u}$ with respect to eq. 1 where $\boldsymbol{c}$ is the velocity vector of the circumferential velocity component $\boldsymbol{c}_u$ and the meridian component $\boldsymbol{c}_m$. However, $\boldsymbol{c}_{1,u}$ is supposed to be zero in further assumptions.

$$\boldsymbol{c} = \boldsymbol{u} + \boldsymbol{w} \tag{1}$$

The velocity at the outlet of the impeller $\boldsymbol{c}_2$ has a clear circumferential component $\boldsymbol{c}_{2,u}$. The difference of the circumferential velocity components at inlet and outlet indicate the power P_{fl} transferred from the impeller to the fluid according to eq. 2.

$$P_{fl} = \dot{m}\left(u_2 c_{2,u} - u_1 c_{1,u}\right) = \dot{m}\, u_2 c_{2,u} \tag{2}$$

Due to this circumferential velocity component the kinetic energy of the outlet air flow is high in comparison to the minimum necessary energy. This amount will be dissipated into heat if it can not be used to increase the static pressure rise at the outlet by appropriate deceleration of the flow in the circumferential direction. One measure is the installation of outlet guide vanes (fig. 2 (mid)). By matching the velocity components with the guide vanes design, the circumferential component is converted into static pressure. The assembly of guiding vanes is of advantage for efficiency and static pressure rise but at the cost of increased installation space. If an even higher pressure rise at a good efficiency is mandatory for the planned fan installation, the replacement of non-rotating guide vanes by a rotating impeller might be an appropriate option. In the same manner as at the first impeller, the second impeller is capable of increasing the power transferred to the fluid. The respective velocity components are shown in fig. 2 (bottom).

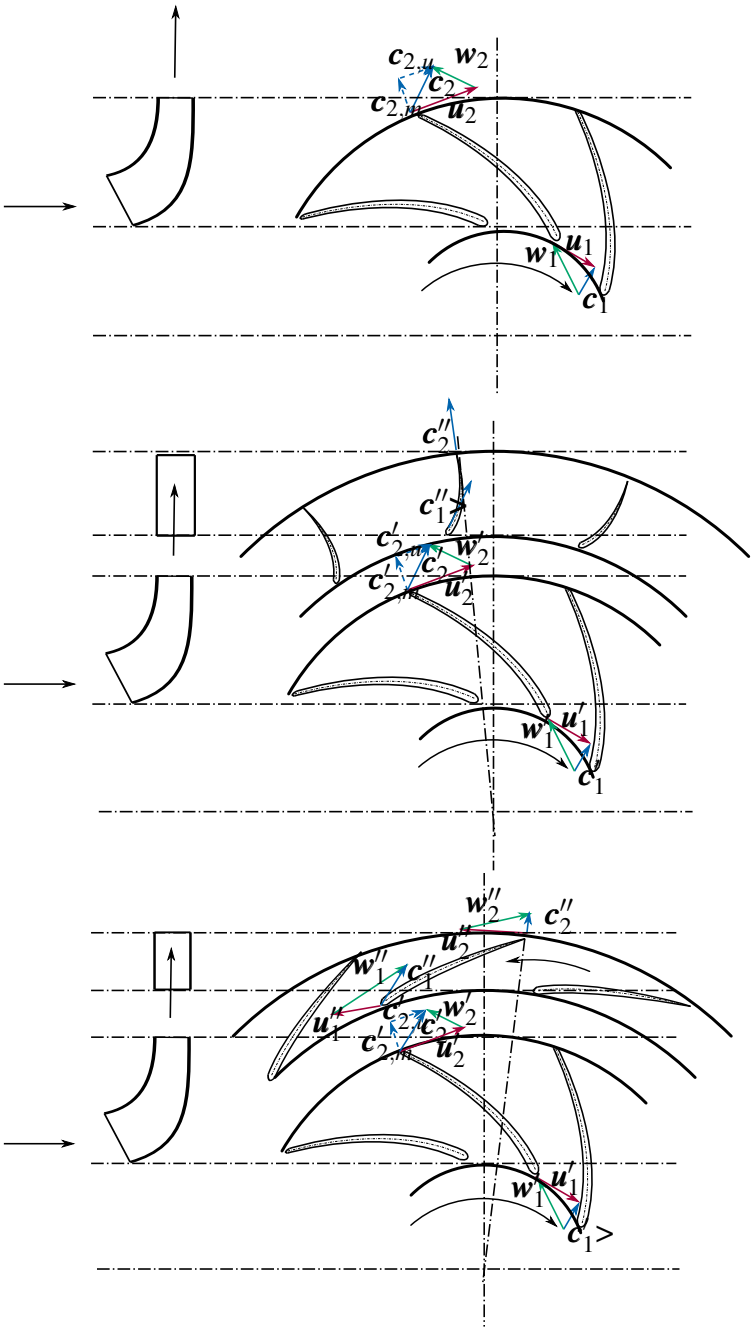

Figure 2: Velocity representation at a centrifugal fan without volute (top), a centrifugal fan with outlet guiding vanes (mid) and a contra-rotating centrifugal fan (bottom)

Parameter	**unit**	**A**	**B**	**CRF**
max. diameter D	mm	120	150	150
flow rate Q	m^3h^{-1}	150		
density ρ	kgm^{-3}	1.2		
pressure rise Δp_{stat}	Pa	125	80	205
el. power cons. P_e	W	15	10	25
rot. speed $n = 0.5\,(n_A + n_B)$	min^{-1}	3000	1500	2250*
flow coefficient $\phi = \frac{4Q}{\pi D^2 u}$	–	0.195	0.200	0.133
work coefficient $\psi = \frac{2\Delta p_t}{\rho u^2}$	–	0.587	0.962	1.096
performance coefficient $\lambda = \phi\,\psi$	–	0.115	0.192	0.146
diameter coefficient $\delta = \psi^{0.25}\phi^{-0.5}$	–	1.98	2.21	2.80
run number $\sigma = \phi^{0.5}\psi^{-0.75}$	–	0.659	0.461	0.341
spec. speed $n_q = nQ^{0.5}\frac{\Delta p}{\rho g}^{0.75}$	min^{-1}	104	73	54

Table 1: Design point definition, main dimensions and dimensionless numbers

DESIGN AND MANUFACTURING

The applied design process is modular for each impeller but also within each impeller for different design steps. It takes the operating point and turbomachinery theory into account instead of pure geometric information. The design of each impeller is divided into the following steps:

1. Design point definition with pressure rise as a ratio of the overall pressure difference, rotational speed of the impeller and direction of rotation (contra-rotating or not).
2. Definition of main dimensions consisting of hub and shroud diameters at meridional inlet and outlet
3. Meridional contour design
4. Definition of number of blades and general blade shape, definition of blade angles at leading and trailing edge
5. Camber line design and application of certain thickness distributions as well as leading and trailing edge shaping
6. 3d-generation of the blades including fillet and material solid generation

According to step 1 the design of the CRF starts with the definition of the design point for both impellers. For the applied design approach only the gas density is needed as the flow can be considered as in-compressible. The design point and the main dimensions according to step 2 are presented in tab. 1. The initial settings of the interactive impeller design approach are proposed by CFturbo and are based on latest turbomachinery design theory. Balance equations are solved together with the application of empirical co-relations, which are given with respect to the specific speed n_q.
Once the parameters have been chosen different values are provided for information. This may be used to check and revise the draft of the fan during the interactive design. Also, based on the design point and impeller diameter, mid span estimations are provided for all velocity components (see fig. 3). Design step 4 is the most important as it defines the blade angles at each span. This determines the power transmission from the fan to the fluid. Camber line design together with thickness distribution

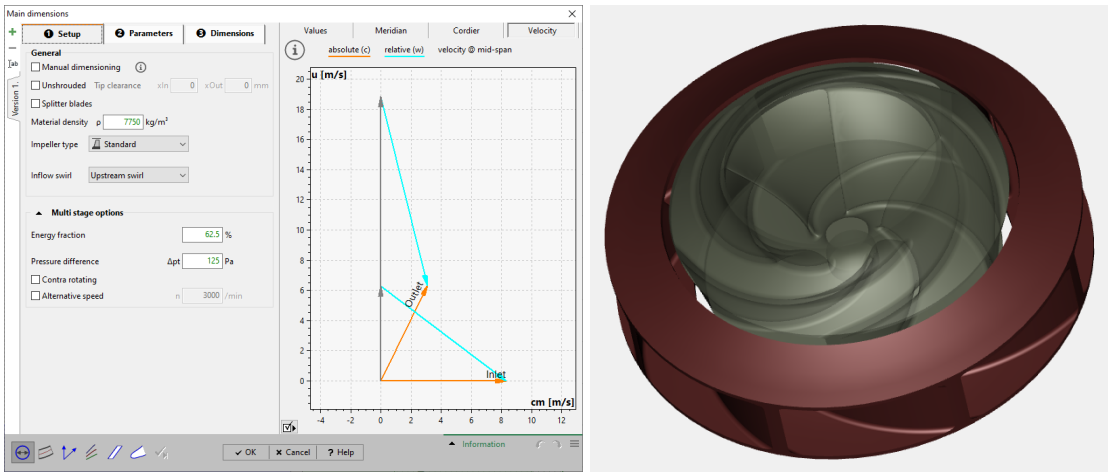

Figure 3: Main dimension of first impeller

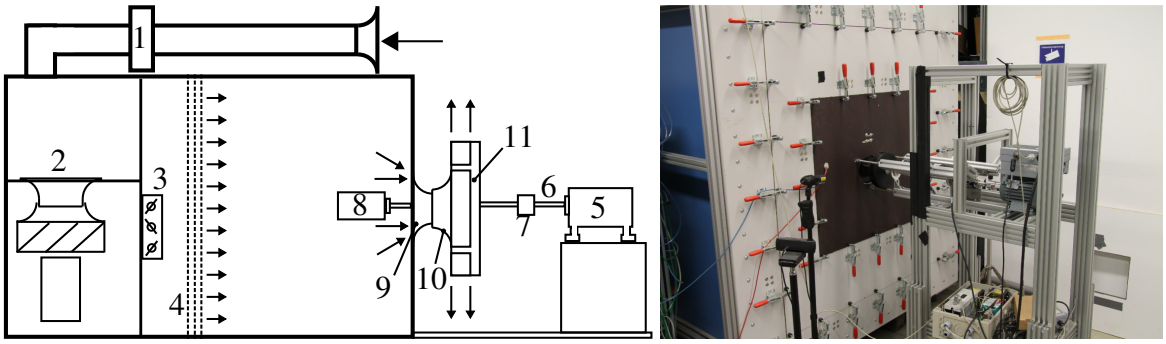

Figure 4: left: test rig according to ISO 5801 with the chamber installed at the suction side of the fan, right: installation of fan at test rig, pressure side view

and leading and trailing edge shaping are necessary before the 3D geometry of the surfaces of the impellers will be generated. The geometric description of the impeller is parametric in a way that any parameter change is followed by an update procedure that yields the new adjusted 3D geometry without any further interaction. The CRF obtained by using CFturbo is displayed in fig. 3.
This design was printed with a 3d-printer (Fused Deposition Modelling) in ABS. Due to several reason the diameter of Impeller B had to be extended to 180 *mm* instead of the design value of 150 *mm*.

EXPERIMENTAL INVESTIGATION

The characteristics measurements were carried out with a test rig according to ISO 5801 as illustrated in fig. 4 (left). The pressure loss due to the volume flow rate measurement (1) is compensated for by an auxiliary fan (2). The additional flap (3) throttles the air flow in order to measure the maximum static pressure of the fan. The flow straightener (4) leads to a uniform velocity distribution at the fan's inlet nozzle (9). Impeller A (10) is directly driven by a 24 V / 200 W DC motor (8) and Impeller B (11) by an AC-motor(5) via shaft (6). The rotational speeds of both impellers were recorded with two separate rpm-counters. The electrical power consumption of Impeller A is measured via voltage and current of the DC motor whilst the consumption of Impeller B is checked with a torque-meter (7). A representation of the installation is shown in fig. 4 (right).
The characteristics of the flow conditions at the outlet as well as at the intersection of Impellers A and B are of special interest. Therefore a laser-optical flow measurement setup comprising a laser and two cameras was utilised to obtain that information.

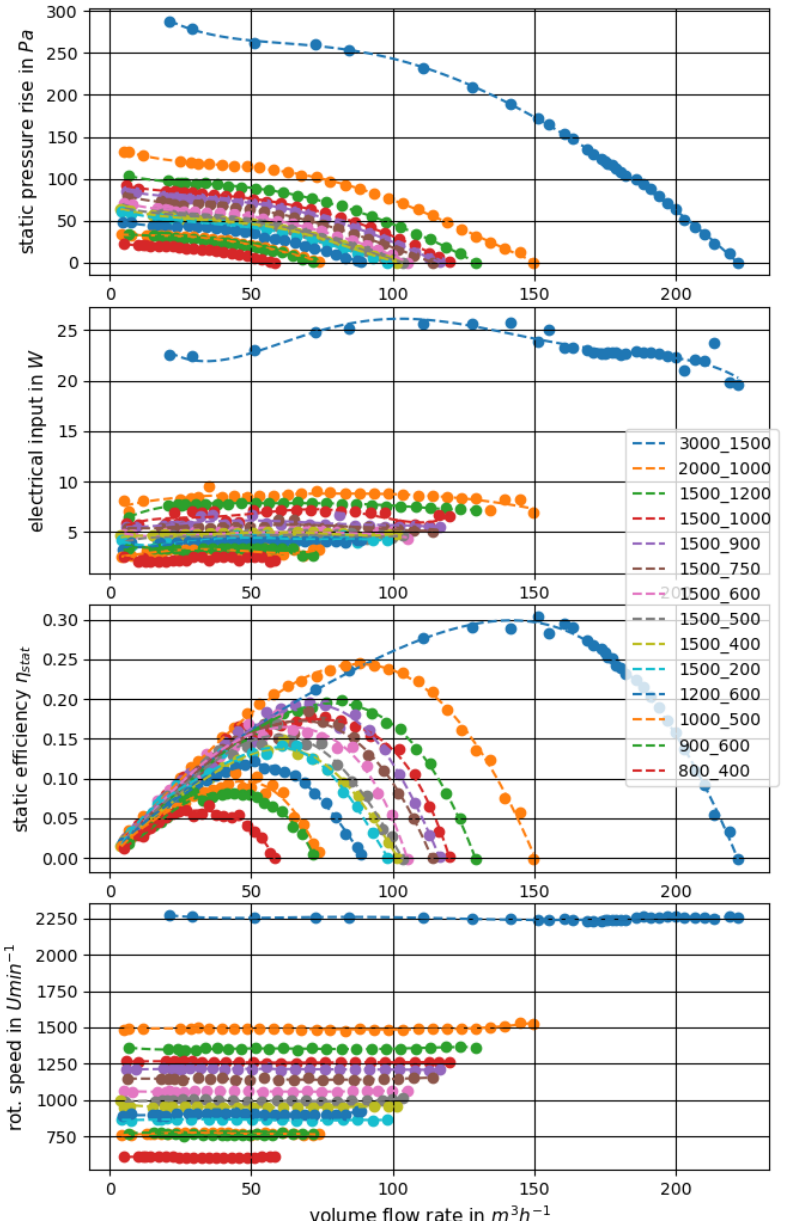

Figure 5: characteristics curve

RESULTS

The measurement results for different rotational speeds at both impellers are shown in fig. 5. For better comparison the characteristics can be represented by the flow coefficient ϕ and the pressure number ψ. The outcome is illustrated in fig 6. The measured velocity distributions clearly prove the dependency of the circumferential velocity component by the ratio of the rotational speeds of both impellers. An extract of the results is represented by fig. 7. The velocity $\boldsymbol{c}''_{2,u}$ almost diminishes for the ratio of 1500:400 at the best efficiency point whilst it is negative (in direction of Impeller A) for lower ratios and positive for higher ratios (in direction of Impeller B).
Additionally, we measured the conditions for different points at the characteristic curve. The results for the best efficiency point and the point of maximum volume flow are depicted in fig. 8.

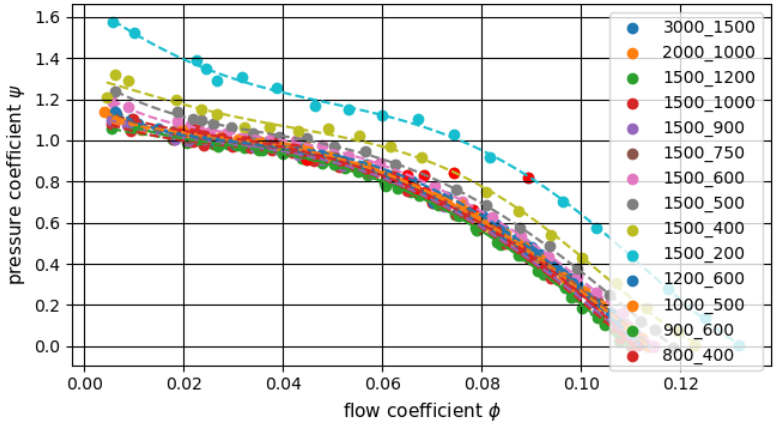

Figure 6: characteristics curve with $\psi = f(\phi)$

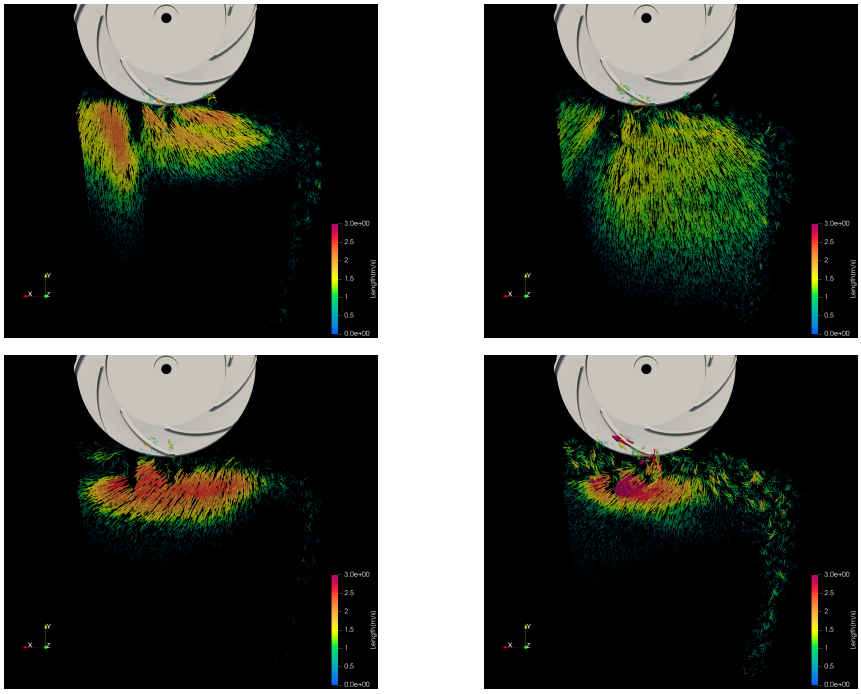

Figure 7: flow conditions at the outlet of the fan, from left to right and top to bottom: 1500-200, 1500-400, 1500-750, 1500-1200 min^{-1}

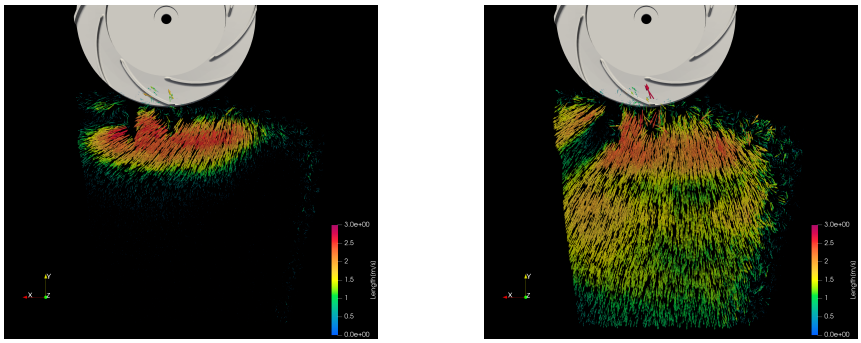

Figure 8: flow conditions at the outlet of the fan, left: 1500 -750 min^{-1} *at best efficiency point, right: 1500 -750* min^{-1} *at max. volume flow rate*

Parameter	**unit**	**design**	**result**
diameter D	mm	150	180
volume flow rate Q	m^3h^{-1}	150	132
stat. pressure rise Δp_{stat}	Pa	205	226
elect. power consumption P_e	W	25	28
rotational speed n	min^{-1}	3000 / 1500	3000 / 1500
flow coefficient ϕ	–	0.133	0.068
work coefficent ψ	–	1.096	0.839
performance coefficent λ	–	0.146	0.057
diameter coefficent δ	–	2.80	3.67
run number σ	–	0.341	0.297
spec. speed n_q	min^{-1}	54	47
stat. efficiency η_{stat}	%	34	30

Table 2: Comparison of results with design criteria

SUMMARY, CONCLUSIONS AND OUTLOOK

In the previous sections, the design and investigation of a contra-rotating centrifugal fans was described. This type of a conventional centrifugal fan comprises two impellers rotating counter-wise at the same axis. The merdional velocity-component at the outlet of the fan is of advantage for static pressure rise, efficiency and performance coefficient as well as for the flow conditions at the inlet side of subsequent devices.
The prototype of the designed fan was 3d-printed and investigated in terms of specification curves and flow conditions. A comprehensive overview of the results obtained by experimental investigation is provided in tab. 2. The shift of several coefficients from design to result is caused by the increased fan diameter. Furthermore the surface of the 3d-printed prototype is not as smooth as it should be for a market-ready fan. This causes a slightly higher friction and pressure loss at the blades. In addition, the chosen setup of two independent motors and the installed bearings are not perfect in terms of power transmission to the impellers. This setup was applied to achieve a good accessibility to both impellers. Based on the findings of this report, a later prototype will be designed in a adapted manner. The result further indicate that Impeller A and B are not in perfect match in terms of their flow characteristics. Therefore the design needs to be revised thoroughly to match Impeller B to the outlet conditions of Impeller A (fig. 9, left). Further investigations have to be performed to improve the losses due to improper sealing between Impeller A and Impeller B. The measurements at the current version without sealing according to fig. 9 (right) show a clear leakage.

ACKNOWLEDGEMENTS

The authors are grateful for the contributions of Hui Jiang, Phillip Mahr, Kai Hermann, Marcus Tietze and Jan Godau (in historical order) to this work. This project was granted by the German Federal Ministry of Economic Affairs under no. 49MF180105.

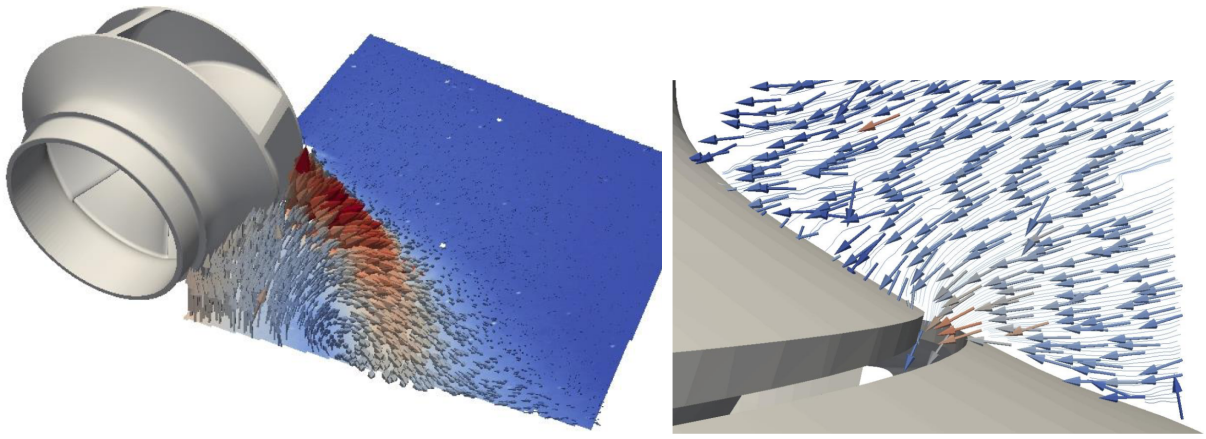

Figure 9: left: velocity at the outlet of impeller A at 3000 min^{-1} and 145 Pa; right: flow conditions at the intersection between Impeller A and Impeller B

BIBLIOGRAPHY

[1] T. Carolus, *Ventilatoren - Aerodynamischer Entwurf, Schallvorhersage, Konstruktion*. Jan. 2013, ISBN: 978-3-8348-2471-4. DOI: 10.1007/978-3-8348-2472-1.

[2] C. Friebe and R. Krause, "Einfluss der einbaubedingungen auf die strömung und die akustik," in *6. VDI Fachtagung Ventilatoren,16.-17.11.2010, Braunschweig*, 2010.

[3] J. Wang, F. Ravelet, and F. Bakir, "Experimental comparison between a counter-rotating axial-flow fan and a conventional rotor-stator stage," Apr. 2013.

[4] T. Lengyel, C. Voß, T. Schmidt, and E. Nicke, "Design of a counter rotating fan - an aircraft engine technology to reduce noise and co2-emissions," Jan. 2009.

[5] M. Heinrich, C. Friebe, and R. Schwarze, "Experimental and numerical investigation of a gearless one-motor contra-rotating fan," *Journal of Power and Energy*, pp. 1–10, 2016. DOI: DOI: 10.1177/0957650916633014. [Online]. Available: pia.sagepub.com.

[6] R. Krause and C. Friebe, "Axial-kompaktlüfter mit hoher leistungsdichte," in *23. Internationale Wissenschaftliche Konferenz, 05.-06.11.2014, Mittweida*, 2014. DOI: 10.13140/2.1.1127.1366.

[7] O. Velde, C. Friebe, and M. Korfanty, "Design and optimisation of contra-rotating fans (presentation)," *Symposium on Innovative Simulations in Turbomachinery*, 2017. DOI: 10.13140/RG.2.2.16004.42883. [Online]. Available: https://www.researchgate.net/publication/321490733_Design_and_Optimization_of_Contra-Rotating_Fans?channel=doi&linkId=5a2549fd4585155dd41ef5bf&showFulltext=true.

[8] C. Friebe, O. Velde, R. Krause, and K. Hackeschmidt, "Design and investigation of a multistage axial contra-rotating fan," *FAN 2018; International Conference on Fan Noise, Aerodynamics, Applications and Systems, 18. - 20.04. 2018, Darmstadt, Germany*, pp. 1–12, 2018.

[9] A. Dreiss, R. Farooqi, J. Friedrichs, and S. Tosin, "Rotating diffusor pump," WO002015084926A1, 2014.

[10] S. Tosin, J. Friedrichs, and A. Dreiss, "New design approach for a highly loaded counter-rotating mixed-flow pump in cavitation conditions," *Proceedings of 11thEuropean Conference on Turbomachinery Fluid dynamics & Thermodynamics ETC11, March 23-27, 2015, Madrid, Spain*, 2015.